Surface Science 668 (2018) 134–143

Contents lists available at ScienceDirect

Surface Science

journal homepage: www.elsevier.com/locate/susc

A structural investigation of the interaction of oxalic acid with Cu(110)

T.W. White[a], D.A. Duncan[b,c], S. Fortuna[d], Y.-L. Wang[e], B. Moreton[a], T.-L. Lee[c], P. Blowey[f], G. Costantini[a], D.P. Woodruff[f,*]

[a] Chemistry Department, University of Warwick, Coventry, CV4 7AL, UK
[b] Technische Universität München, Physik Department E20, Garching, D-85748, Germany
[c] Diamond Light Source, Didcot, OX11 0DE, UK
[d] SISSA, Via Bonomea 265, Trieste, Italy
[e] Institute of Physics & University of Chinese Academy of Sciences, Chinese Academy of Sciences, Beijing 100190, China
[f] Physics Department, University of Warwick, Coventry, CV4 7AL, UK

A B S T R A C T

The interaction of oxalic acid with the Cu(110) surface has been investigated by a combination of scanning tunnelling microscopy (STM), low energy electron diffraction (LEED), soft X-ray photoelectron spectroscopy (SXPS), near-edge X-ray absorption fine structure (NEXAFS) and scanned-energy mode photoelectron diffraction (PhD), and density functional theory (DFT). O 1s SXPS and O K-edge NEXAFS show that at high coverages a singly deprotonated monooxalate is formed with its molecular plane perpendicular to the surface and lying in the [1$\bar{1}$0] azimuth, while at low coverage a doubly-deprotonated dioxalate is formed with its molecular plane parallel to the surface. STM, LEED and SXPS show the dioxalate to form a (3 × 2) ordered phase with a coverage of 1/6 ML. O 1s PhD modulation spectra for the monooxalate phase are found to be simulated by a geometry in which the carboxylate O atoms occupy near-atop sites on nearest-neighbour surface Cu atoms in [1$\bar{1}$0] rows, with a Cu–O bondlength of 2.00 ± 0.04 Å. STM images of the (3 × 2) phase show some centred molecules attributed to adsorption on second-layer Cu atoms below missing [001] rows of surface Cu atoms, while DFT calculations show adsorption on a (3 × 2) missing row surface (with every third [001] Cu surface row removed) is favoured over adsorption on the unreconstructed surface. O 1s PhD data from dioxalate is best fitted by a structure similar to that found by DFT to have the lowest energy, although there are some significant differences in intramolecular bondlengths.

1. Introduction

It is well-established that carboxylic acids deprotonate when adsorbed on many metal surfaces, and notably on Cu(110), which has proved to be the model surface used in many of these studies. Indeed, more generally, carboxylate-substrate bonding is widely used to tether a range of molecules to surfaces (e.g. [1]). The presence of the formate species HCOO, the deprotonated form of the simplest carboxylic acid, formic acid (HCOOH, FoA – see Fig. 1), on Cu(110) was first inferred by Wachs and Madix in temperature-programmed reaction spectroscopy (TPRS) from a pre-oxidised Cu(110) surface exposed to methanol [2]. Subsequently Ying and Madix [3] deduced from TPRS that surface formate is formed by exposure of Cu(110) to formic acid. Spectroscopic observation of the formate species on Cu(110) was subsequently achieved with both ultraviolet and X-ray photoelectron spectroscopy (UPS and XPS) [4], high-resolution electron energy loss spectroscopy (HREELS) [5] and reflection-absorption infrared spectroscopy (RAIRS) [6]. While these spectroscopic studies clearly indicated that formate is bidentate bonded to the surface through the two (equivalent) O atoms, with the molecular plane perpendicular to the surface, it was ultimately scanned-energy mode photoelectron diffraction (PhD [7]) that provided a detailed quantitative description of the local bonding geometry [8,9]. Specifically, the molecule is adsorbed in a short bridge site on Cu(110), the molecular plane lying in a [1$\bar{1}$0] close-packed direction on the surface, with the two O atoms almost exactly atop two nearest-neighbour surface Cu atoms (Fig. 2).

Subsequently, a surface acetate species, formed by deprotonation of acetic acid (AA, Fig. 1) exposed to the Cu(110) surface, was identified spectroscopically [10–12] and shown to have its carboxylate plane lying in a ⟨110⟩ azimuth with its C–C axis perpendicular to the surface, while a PhD investigation [13] identified the local bonding site to be the same as for the formate species. A third simple carboxylate, namely benzoate formed by the deprotonation of benzoic acid (BA, Fig. 1) on Cu(110), was characterised by HREELS, RAIRS, low energy electron diffraction (LEED) and scanning tunnelling microscopy (STM) [14–16] showing that at low coverages the phenyl ring of the benzoate is essentially parallel to the surface, but at high coverage the molecule stands up. A PhD investigation of this standing-up phase [17] found the local bonding geometry on Cu(110) to be identical to that of formate and acetate. The molecular orientation was also confirmed by electron-stimulated desorption ion-angular distributions (ESDIAD) [18]. STM studies indicate that Cu adatoms may be associated with the benzoate species, at least at low-coverages [19–21], forming benzoate dimers with an intermediate Cu adatom or clusters of four benzoate molecules around a pair of Cu

* Corresponding author.
E-mail address: d.p.woodruff@warwick.ac.uk (D.P. Woodruff).

https://doi.org/10.1016/j.susc.2017.10.025
Received 19 September 2017; Received in revised form 23 October 2017; Accepted 26 October 2017
Available online 28 October 2017

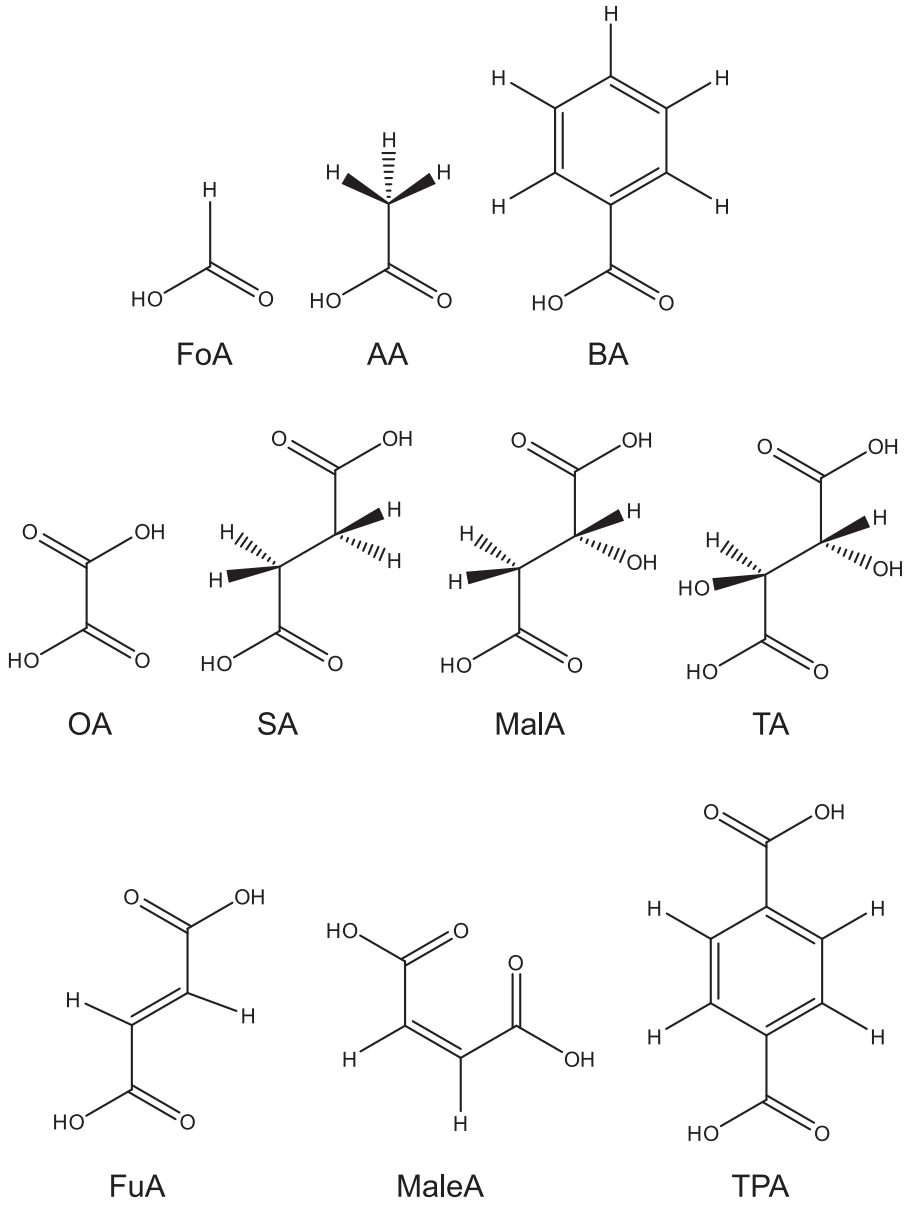

Fig. 1. Schematic diagrams of the carboxylic acids discussed in the text, namely: formic acid (FoA), acetic acid (AA), benzoic acid (BA), oxalic acid (OA), succinic acid (SA), malic acid (MalA), tartaric acid (TA), fumaric acid (FuA), maleic acid (MaleA) and terephthalic acid (TPA).

adatoms. However, at least for the high-coverage phases, the local bonding geometries of all these simple deprotonated single-carboxylic acid group molecules are identical and show no evidence for any influence of Cu adatoms.

Interesting questions arise, however, regarding the behaviour of dicarboxylic acids. Are they singly or doubly deprotonated, and what it is the local bonding geometry? Here we seek to answer these questions for the simplest dicarboxylic acid, oxalic acid. Interestingly, there have already been a number of investigations of several more complex dicarboxylic acids, shown in Fig. 1, motivated in large part by interest in the interaction of chiral molecules (and related non-chiral species) on surfaces [22]. For several of these molecules, namely tartaric acid, TA [23,24], succinic acid, SA [25], and malic acid, MalA [26], the results of mainly STM and RAIRS studies indicate that the molecules are doubly-deprotonated and adopt a lying-down configuration at low coverage, but are singly deprotonated and stand up at higher coverages. Moreover, low coverage STM and XPS studies of terephthalic acid, TPA, on Cu(110) clearly indicate a doubly-deprotonated lying-down species in several different ordered phases [27], while a RAIRS study indicates that at higher coverage a singly-deprotonated standing-up phase occurs [28]; the general behaviour of TPA therefore seems to be similar to that of tartaric, succinic and malic acids. This behaviour implies that as the coverage increases some doubly-deprotonated molecules are re-protonated, presumably by H atoms coming from the (single) deprotonation of the newly-arriving acid molecules. The only detailed quantitative structural investigation of any of these dicarboxylic acid adsorbates is a PhD investigation of the tartaric acid system [29] which concluded that the monotartrate stands up (albeit with some tilting) with a local bonding geometry essentially identical to that of formate, acetate and benzoate (Fig. 2). Even in the lying down bitartrate phase the bonding of the two carboxylate groups to the Cu surface is closely similar, with O atoms in near-atop sites of adjacent pairs of Cu atoms in the $[1\bar{1}0]$ azimuth, although there is some offset from the ideal aligned short bridge site adopted by formate (Fig. 2). This local distortion is clearly a consequence of the mismatch of O–O between the two carboxylates and Cu–Cu spacing in the [001] azimuth on the (110) surface; similar effects

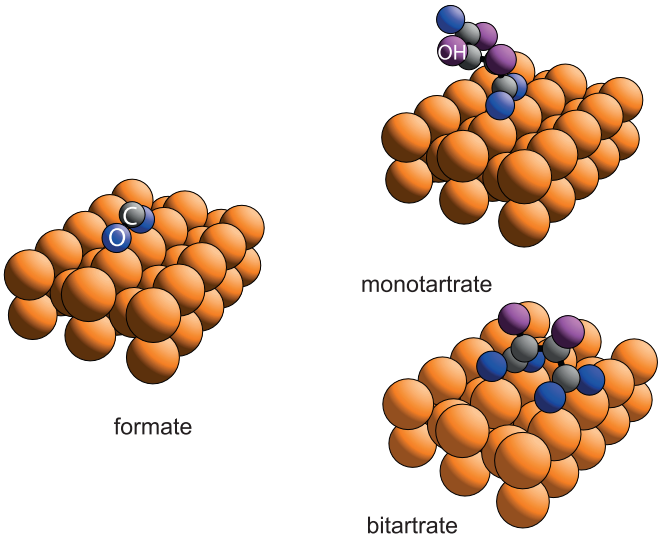

Fig. 2. Schematic diagrams showing the local adsorption geometries previously reported for the formate, monotartrate and bitartrate species on Cu(110) based on PhD investigations. Note that the PhD technique is insensitive to the location of H atoms, so these are omitted from the diagrams. OH species are represented by the associated O atoms with a different colouring. (For interpretation of the references to colour in this figure legend, the reader is referred to the web version of this article.)

having been seen for the simple deprotonated amino acids glycinate and alanate, in which bonding to the surface is not only by the carboxylate O atoms but also the amino N atom [30,31].

Rather different behaviour has been reported for the interaction of maleic acid (MaleA) and fumaric acid (FuA), with the application of STM, LEED and RAIRS together with C 1s XPS, leading to the conclusion that maleic acid is always doubly deprotonated on Cu(110) [32] whereas fumaric acid is only detected (with RAIRS) as a singly deprotonated species on this surface [33]. These two acid molecules are the *cis* and *trans* form of butenedioic acid, and while the conclusion regarding maleic acid may be attributable to the *cis* conformation of the molecule it is not clear why the *trans* conformation of fumaric acid should preclude the possibility of it being doubly deprotonated.

The only previous study of oxalic acid on Cu(110) appears to be that of Martin, Cole and Haq [34] who concluded, on the basis of RAIRS data, that the molecule stands up and is singly deprotonated (monooxalate). At low exposures no absorption bands could be detected; however, this could be consistent with the presence of a lying-down (presumably doubly deprotonated - dioxalate) species in which the molecular vibrational modes would not be dipole active and thus cannot be detected in RAIRS. An investigation of oxalic acid interaction with Cu(111), using STM and high-resolution soft (synchrotron radiation) XPS (SXPS), indicated that both mono- and di- oxalate species occurred, primarily at low and high coverage respectively [35].

Here we report the results of experiments conducted to obtain a rather complete understanding of the structural and chemical properties of the surface species resulting from exposure of Cu(110) to oxalic acid. Basic characterisation of the system was achieved through the use of STM, LEED, and SXPS, particularly from the O 1s state. Quantitative structural information has been obtained from O 1s PhD combined with O K-edge NEXAFS (near-edge X-ray absorption fine structure). We find that oxalic acid follows the pattern of most other (more complex) dicarboxylic acids in adopting a doubly deprotonated lying-down oxalate at low coverage but a singly deprotonated standing-up species at high coverage. The PhD data provide a clear determination of the local adsorption geometry for the monooxalate, but identifying the exact geometry of the dioxalate proved more challenging. However, STM images of the (3×2) phase led indirectly to the possibility that this phase involves [001] missing rows, and DFT calculations confirm that the dioxalate is more strongly adsorbed on such a reconstructed surface. O 1s PhD data are consistent with the qualitative model favoured by the DFT calculations.

2. Experimental details

Initial characterisation experiments were performed in a UHV surface science chamber based at the University of Warwick, fitted with a LEED optics, a low-temperature STM, and the usual facilities for sample handling and cleaning. The Cu(110) sample was prepared in situ by cycles of 1 keV Ar^+ ion bombardment and annealing to 870 K for 5 min until a clean well-ordered surface was obtained as indicated by LEED and STM. Oxalic acid deposition was by room temperature evaporation from a kovar glass tube attached to the UHV system; during vacuum bake of the metallic components (to only 373 K) this tube was kept close to room temperature to avoid excess material loss due to the high vapour pressure. The tube was then outgassed with a heat gun, purged into the pumping line of the sample load lock.

SXPS, NEXAFS and PhD measurements were made in the UHV surface science end-station of beamline I09 at Diamond Light Source. This beamline is fitted with a pair of canted undulators, each feeding a different monochromator, but both bringing the focussed monochromated beams to the same spot on the sample. The lower-energy undulator radiation branch is fitted with a grazing-incidence plane-grating monochromator capable of providing photons at the sample in the energy range 100–1100 eV. The higher-energy branch, using a double-crystal Si(111) monochromator, was not used in the experiments reported here. Sample cleaning and dosing used the same methods as in the Warwick chamber, although sample ordering and cleanness in this case were assessed using a low-current LEED optics and SXP spectra obtained using a VG Scienta EW4000 electron spectrometer with a $\pm30^\circ$ acceptance angle in the plane of incidence and polarisation of the radiation, mounted within this polarisation plane at an angle of 60° between the incident radiation and the direction from the sample to the centre of the detector. This analyser was also used to collect the photoemission data for the PhD experiments and the Auger electron emission in the NEXAFS studies.

3. Surface characterisation results

3.1. STM and LEED

Initial characterisation of the system using STM and LEED showed that a nominal exposure at room temperature of oxalic acid of 5×10^{-6} mbar s, as measured by an ion gauge within the main chamber, led to a disordered surface with no ordered molecular imaging detectable with STM (Fig. 3(a)). However, after annealing to 398 K both STM and LEED indicated the presence of a (3×2) ordered phase, as shown in Fig. 3(b and d). This was the only ordered phase seen by either technique at any surface coverage. While the protrusions seen in STM image of the (3×2) phase lack any visible internal structure these are tentatively assumed to be due to individual adsorbed molecules. This attribution is supported by SXPS data obtained later (see below), which provided a coverage estimate of a phase giving a (3×2) LEED pattern of approximately 0.2 ML, broadly consistent with one molecule per (3×2) surface unit mesh (0.17 ML). Further support for this interpretation is provided by the STM image of Fig. 3(c), obtained after further annealing to 423 K, which led to a loss of molecules from the surface and produced a disordered surface that does show individual ad-species. In particular, a feature in the centre of the superimposed green circle appears to be an isolated adsorbed molecule in an otherwise clean area of the surface, and indeed the shape of this feature could be consistent with a lying-down fully deprotonated dioxalate molecule that SXPS and NEXAFS data (see below) indicate to be present on the surface in the (3×2) phase.

The STM image of the (3×2) phase (Fig. 3(b)) shows a particularly surprising set of local defects, namely protrusions at the centre of the (3×2) ordered features that appear to be quite similar to those of the

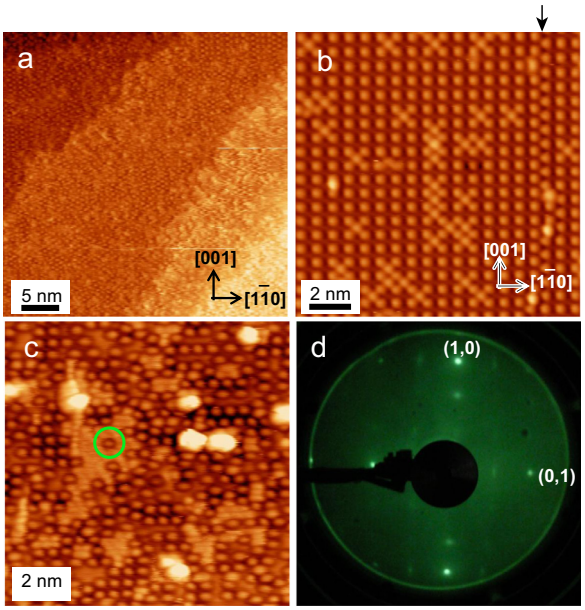

Fig. 3. (a) STM image of the disordered unannealed surface. (b) STM image and (d) LEED pattern recorded at 148 eV from the ordered (3 × 2) phase formed by oxalic acid on Cu(110) following annealing of a higher-coverage disordered phase to 398 K. (c) shows an STM image obtained after further heating to 423 K. Tunnelling conditions: (a) 120 pA, −1.1 V; (b) 180 pA, −1.1 V; (c) 100 pA, 1.1 V.

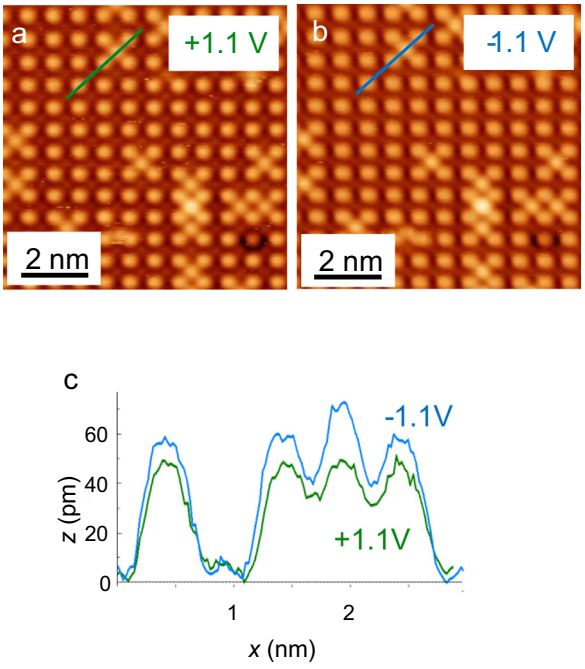

Fig. 4. (a) and (b) show STM images of the (defected) (3 × 2) phase obtained at opposite bias voltages (but the same tunnelling current of 180 pA). (c) shows the line-scan profiles along the equivalent locations in the two images, colour-coded in green and blue. (For interpretation of the references to colour in this figure legend, the reader is referred to the web version of this article.)

un-defected regions. At first sight these could be interpreted as additional identical molecules, but the centre of a (3 × 2) mesh (or any mesh involving an odd-numbered periodicity in one direction) cannot correspond to an identical local site. In fact the apparent height of the centred defect protrusions, relative to those of the regular (3 × 2) protrusions, does depend on the tunnelling conditions (see Fig. 4), with the ratio of these heights being close to 1.0 in positive sample bias (empty surface state imaging), but close to 1.25 in negative sample bias (occupied surface state imaging). This observation is consistent with the view that the molecules giving rise to these two features do differ.

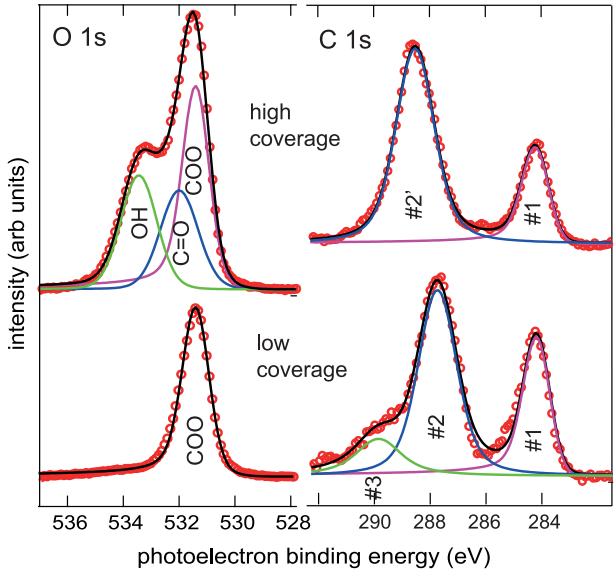

Fig. 5. SXP spectra around the O 1s and C 1s emission peaks recorded from the two different coverages of oxalic acid species on Cu(110).

Notice that the STM image of Fig. 3(b) also shows another defect structure, namely an antiphase domain boundary close to, and running parallel to, the right-hand edge of the image, marked with an arrowhead. Images (not shown) from less well-ordered preparations show a much higher density of these antiphase domain boundaries to produce a 'striped' structure that led to LEED patterns with spot splitting of (n × 2) character where n is significantly larger than 3. Notice, though, that the width of the antiphase domain boundaries appears to correspond to twice the Cu–Cu atom spacing along [1$\bar{1}$0] so all molecules on both sides of these boundaries occupy identical local sites.

3.2. SXPS and NEXAFS

Sample preparation for the experiments performed at Diamond followed essentially the same recipes used in Warwick, but comparison of the O 1s and Cu 2p SXP spectra provided estimates of the associated coverages. For the initially-deposited high-coverage phase and the lower-coverage annealed phase SXPS led to coverage estimates of 0.35 ML and 0.20 ML, respectively. As remarked above, the lower coverage phase yielded a (3 × 2) LEED pattern that, for one molecule per surface unit mesh (as implied by the STM images) would correspond to a coverage of 0.17 ML, consistent with the SXPS estimate. No ordered phase LEED pattern was obtained from the higher-coverage preparation; published density functional theory (DFT) calculations for a mono-oxalate phase were based on (2 × 2) ordering with a coverage of 0.25 ML [36] but a c(2 × 2) ordering with a coverage of 0.5 ML would also appear to be possible (and was reported by Martin et al. [34]). The SXPS-derived coverage lies between these two values.

O 1s and C 1s SXP spectra from the two different surface coverages are shown in Fig. 5, recorded at photon energies of 700 eV and 400 eV, respectively. The single narrow peak in the O 1s spectrum recorded from the low-coverage phase clearly indicates that all O atoms are locally-equivalent, implying that in this phase the molecule is doubly deprotonated and hence is most probably lying flat on the surface. By contrast, the O1s spectrum from the high-coverage phase clearly contains at least two distinct chemically-shifted components, one of which has a photoelectron binding energy closely similar to that of the deprotonated oxygen atoms in the low-coverage phase, while the other, at a higher

binding energy, may be attributed to emission from a carboxylic moiety that is still protonated; we may therefore infer that this spectrum is from a monooxalate species. Such a species must give rise to three chemically-distinct O 1s components corresponding to the O atoms of deprotonated COO and the OH and C=O components of the intact acid group. A unique unconstrained three-component fit to this spectrum is not possible, and the fit shown in Fig. 5 (using Doniach-Sunjic lineshapes) is based on the assumption that the COO component has exactly the same binding energy and spectral width as that seen in the spectrum from the low-coverage di-oxalate spectrum, while the other two components, each have an integrated intensity that is approximately one half of that of the COO component. These constraints would be consistent with a surface being covered by a standing-up monooxalate species. Notice that with these constraints applied the resulting fit shown in Fig. 5 has the OH and C=O Gaussian peak widths being approximately twice that of the COO peak; the origin of this effect is unclear although the O atoms in the OH and C=O components do have a very different electronic environment away from the surface to that of the O atoms in the COO that are bonded to the surface.

As a further aid to the identification of the three components, DFT calculations of the chemical shifts to be expected from this mono-oxalate species were performed using the CASTEP code [37], assuming a c(2 × 2) ordering of the (structurally-optimised) mono-oxalate species, but with a single core hole in a c(6 × 6) unit mesh to minimise hole-hole interactions in the calculation. These calculations led to estimated chemical shifts relative to the COO component of 0.02 eV and 1.9 eV for the C=O and OH components, respectively. This clearly indicates that the component with the highest binding energy is from the OH oxygen atom, while the intermediate component, with only a small energy shift from the COO component, corresponds to the C=O component. The corresponding chemical shift values (for the C=O and OH components) used in the experimental fit of Fig. 5 are 0.6 eV and 2.1 eV with relative intensities of COO:C=O:OH of 1:0.58:0.64. However, fits to this spectrum proved particularly insensitive to the relative binding energy of the C=O component and reasonable fits could also be obtained with a much smaller chemical shift of the C=O component of 0.2 eV, much closer to the DFT-predicted value. A consistent trend of all of these fits was that the relative intensity of the COO component was lower than that to be expected from the molecular stoichiometry; this is consistent with attenuation of this component due to inelastic scattering of the photoelectrons passing through the upper part of the molecular layer.

This apparently straight-forward interpretation of the O 1s spectra in terms of monooxalate and dioxalate species at high and low coverages would lead one to expect a single C 1s component from the low coverage phase, while from the high coverage phase there may be two components with a splitting due to differences between the COO and COOH carbon atom environments (in formate and formic acid on Cu(110) a difference of ~2 eV has been reported with individual values of 287.5–288.0 eV and 289.6–290.0 eV, respectively [38,39]). In fact the high-coverage phase shows two dominant peaks at photoelectron binding energies of 284.1 eV and 288.5 eV, while the low-coverage spectrum has three components at energies of 284.1 eV, 287.7 eV and 289.9 eV. This behaviour with simple 'clean' O 1s spectra and complex multi-peak C 1s spectra has also been reported for oxalic acid interaction with Cu(111) by Faraggi et al. [35]. The peak at 284.1 eV labelled #1 in Fig. 5 is consistent with the presence of graphitic carbon. In other experiments we have conducted of oxalic acid on Cu(111) this peak can dominate the spectrum with a graphitic carbon coverage estimate significantly in excess of 1 ML, only consistent (in the presence of coadsorbed oxalate peaks) with the presence of three-dimensional islands of graphitic material. As this peak only appeared after oxalic acid deposition it must clearly result from some kind of decomposition reaction on the surface. However, perhaps surprisingly, we found no evidence for this peak to increase with continued exposure to the incident synchrotron radiation, indicating that it is not due to beam-induced damage. The peaks at 287.7 eV and 288.5 eV (#2 and #2′) must be attributed to C atoms

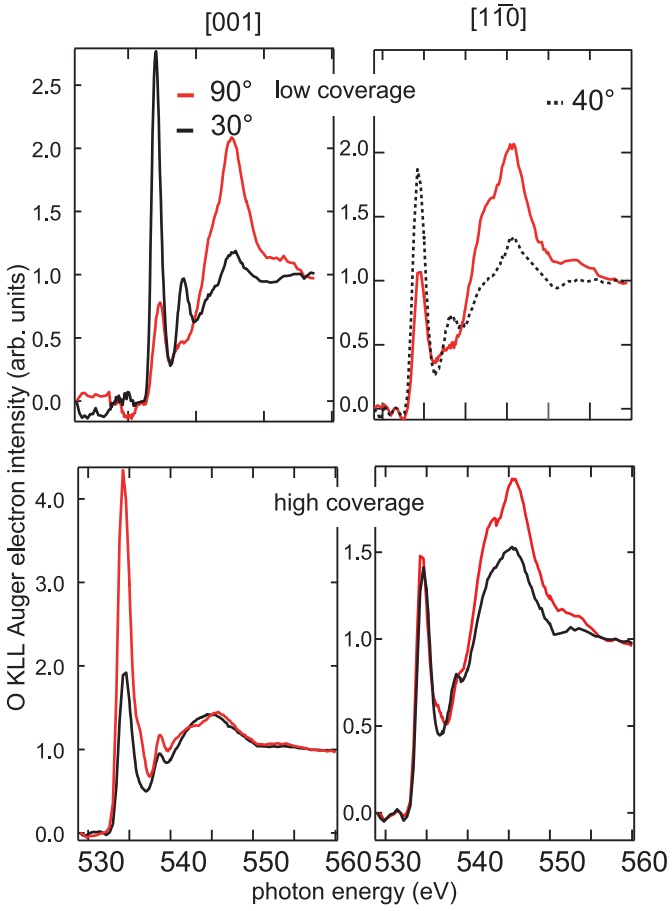

Fig. 6. O K-edge NEXAFS spectra recorded from the low and high coverage phases formed by oxalic reaction with Cu(110), recorded for incidence in two orthogonal azimuthal directions, and at two different incidence angles, defined as the angle between the surface normal and the **A**-vector of the incident radiation. Normal incidence is thus labelled 90°.

within the adsorbed oxalate species. This energy difference between the two phases cannot be attributed to the low coverage peak being due to only COO with the high-coverage peak being due to both COO and COOH species, because the energy shift is of opposite sign to that for the HCOO and HCOOH species reported above. Such an energy shift should also be accompanied by a broadening of the peak from the high coverage phase due to the underlying doublet, but the widths of the two fitted peaks in Fig. 5 are identical. The only plausible explanation for the difference seems to be the very different electronic screening environment of C atoms in a lying-down and standing-up molecule. The origin of the C 1s peak #3 at 289.9 eV is even less clear. Faraggi et al. in their study of oxalic acid on Cu(111) have suggested that this peak may be due to some kind of CO_2 or CO_3 species but these seem unlikely to be stable at room temperature and even less likely to survive the sample annealing. The energy of this feature could correspond to an intact carboxylic acid (as in the value reported for formic acid), but this too, is unlikely to be stable after annealing, while the O 1s spectrum shows no hint of such a species being present from the low-coverage surface. A more probable explanation is that this feature is a shake-up satellite of the carboxylate C peak #2; this assignment of a similar feature in the case of tartaric acid on Cu(110) was found to account for an otherwise non-stoichiometry of the molecule implied by the C 1s XPS [30].

Supporting evidence for the assignment of the low-coverage phase to a lying-down molecule and of the high-coverage phase to a standing-up molecule is provided by the O K-edge NEXAFS data of Fig. 6. These orientations are demonstrated by the dependence of the relative intensity of the sharp peak at a photon energy of approximately 535 eV, due to ex-

citation to a π^*-resonance, on the polarisation direction of the incident radiation. This peak is expected to have its maximum intensity when the **A**-vector of the incident radiation is perpendicular to the molecular plane. Thus in the low coverage phase this intensity is larger at grazing incidence than at normal incidence, consistent with a lying-down configuration. For the high coverage phase the intensity of this feature is greatest when the **A**-vector lies in the surface plane in the [001] azimuth, indicating not only that the molecule stands up, but that the molecular plane lies in the $[1\bar{1}0]$ azimuth. Notice, though, that the π^*-resonance peak does not completely vanish at normal incidence from the low coverage phase, nor at normal incidence in the $[1\bar{1}0]$ azimuth from the high coverage phase, implying a small amount of disorder or tilting and twisting.

4. Structure determination: PhD data, simulations, and DFT calculations

4.1. Introduction

The PhD technique exploits the coherent interference of the directly emitted component of a photoelectron wavefield from a near-surface atom with those components scattered by atoms in the local environment of the emitter. By varying the incident photon energy, the photoelectron kinetic energy (and hence the photoelectron wavelength) is varied, causing the scattered components of the photoelectron wavefield to switch in and out of phase with the directly emitted component. The resulting modulations in the photoemission intensity in a specific direction, as a function of photon energy, provide structural information on the local environment of the emitter. In the present case PhD modulation spectra were obtained by measuring photoelectron energy distribution curves (EDCs) of the O 1s peak(s), at 4 eV steps in photon energy, over the photoelectron kinetic energy range of 50–300 eV, for a range of different polar emission angles in the $[1\bar{1}0]$ azimuth. The 2-D detector fitted to the large acceptance-angle electron spectrometer allowed separate spectra to be extracted at 5° intervals over a 50° polar emission angle range for any specific sample orientation. These spectra were then processed following our general PhD methodology (e.g. [6]) in which the individual EDCs are fitted by one or more Gaussian peaks, a Gauss error function (step), and a template background obtained from the wings of the EDCs. The integrated areas of each of the individual peaks were then plotted as a function of photoelectron kinetic energy, $I(E)$, and used to define a stiff spline, $I_0(E)$, through $I(E)$, that represents the non-diffractive intensity and instrumental factors. The spline was then subtracted from, and used to normalise, the integrated areas, to provide the final PhD modulation spectrum, $\chi(E) = (I(E) - I_0(E))/I_0(E)$.

The results of DFT calculations for the adsorbed monooxalate on Cu(110) have already been published [37]. These calculations, assuming that the PBE exchange correlation suffices to describe the chemisorbed configurations, have shown that vertically standing molecules are energetically favoured allowing for high packing densities.

However, for flat lying geometries the dispersion forces should also be taken into account for an accurate estimation of the adsorption energy and the computational approach used for the new calculations reported here differs from that reported in ref. [37] as here London forces are also accounted for [40]. Specifically calculations were performed with the Perdew–Burke–Ernzerhof generalised gradient-corrected approximation (PBE-GGA) for the exchange and correlation energy functional [41] with added semi-empirical Grimme's DFT-D2 van der Waals interaction correction. The spin-polarized Kohn-Sham equations were solved in the plane wave pseudopotential framework, as implemented in the PWscf code of the Quantum ESPRESSO distribution [42,43] The surface was modelled with a slab consisting of five atomic layers, separated in the z direction by more than 13 Å, with the lattice parameter set to the equilibrium value calculated for the bulk (3.66 Å). The lower-most two layers constrained to their bulk-like coordinates, and energies were calculated using a regular grid of k-points comparable to the $12 \times 14 \times 1$ grid used for the clean Cu(111)(1×1) surface.

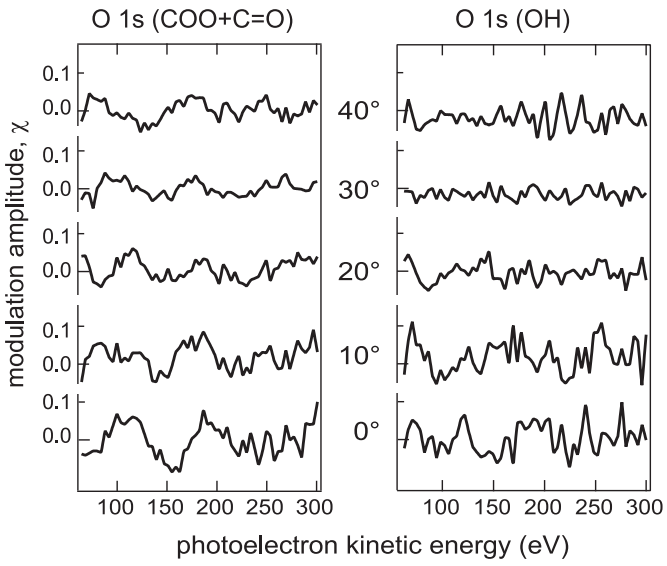

Fig. 7. Experimental PhD modulation spectra at different polar emission angles in the $[1\bar{1}0]$ azimuth recorded from the two fitted components of the O 1s emission from the high-coverage phase produced by oxalic acid reaction with Cu(110).

In general, DFT calculations show that flat-lying fully deprotonated configurations, likely to decompose into CO_2 on the clean copper surface, can be stabilised by the presence of adatoms or surface reconstructions. The formation energy ΔE associated with the process of adsorbing m oxalic acid molecules on a clean copper surface with the release of n hydrogen molecules and the removal of k Cu atoms can be calculated as:

$$\Delta E = E_{\text{tot}} + nE_{\text{H}_2} + kE_{\text{Cu}} - mE_{\text{COOH}_2} - E_{\text{surf}}$$

where E_{tot} is the energy of the assembled system, E_{H_2}, E_{Cu}, E_{COOH_2} are the energies of an isolated molecular hydrogen, a bulk copper atom, and an isolated oxalic acid respectively, while E_{surf} is the energy of the clean unreconstructed surface.

4.2. High-coverage phase

As discussed in Section 3.2, the O 1s SXP spectra from the high coverage phase actually comprise three chemically-shifted components, but there is some uncertainty in the exact value of the chemical shift of the C=O component relative to that from the COO oxygen atoms, although it is clearly small. Inevitably, the signal-to-noise ratios of the angle-resolved spectra, extracted by averaging over only a 5° range, are worse than those of the wide-angle integrated spectra of Fig. 5, so it proved unrealistic to separate all three components in a meaningful fashion, and fits to these PhD EDCs were conducted with only two components, a high binding energy peak corresponding to emission from the OH oxygen atom, and a single low binding energy peak, corresponding to emission from all three of the COO and C=O oxygen atoms. A set of the resulting PhD modulation spectra recorded at 10° intervals in emission angle is shown in Fig. 7.

While quantitative interpretation of such PhD spectra can only be achieved through the use of multiple scattering simulations for different model structures, inspection of the spectra shown in Fig. 7 does allow some immediate conclusion to be drawn. Firstly, none of the spectra recorded for the OH component show any meaningful long-period modulations, but rather are dominated by noise. This would be consistent with a standing up-adsorption geometry as the OH oxygen atom would then be rather far (~4–5 Å) above the strongly-scattering Cu substrate atoms. The modulations observed in the spectra from the combination

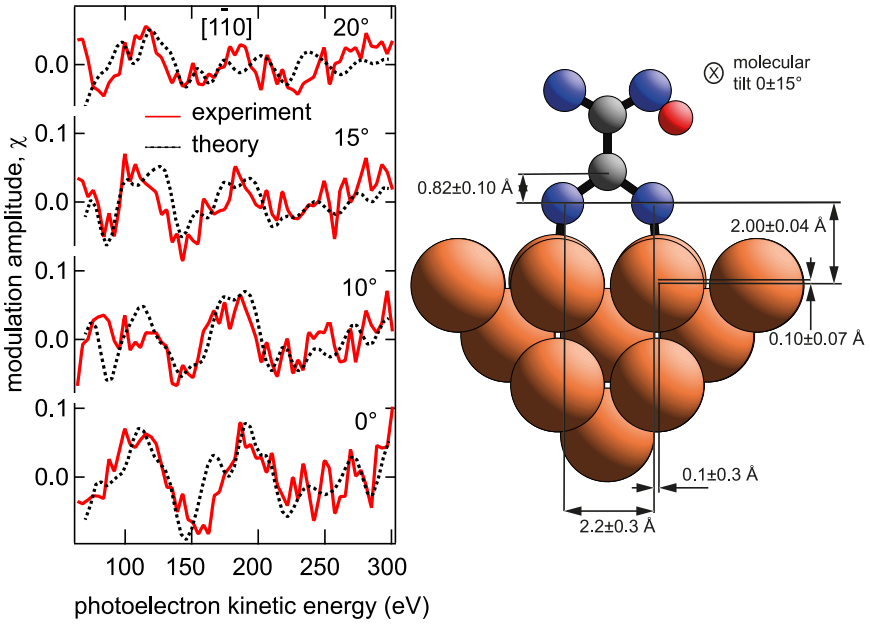

Fig. 8. Comparison of experimental 1s PhD spectra from the low binding energy (COO + C=O) peak from the high coverage phase formed by oxalic acid reaction with Cu(110) with the results of multiple scattering simulations for the best-fit structure. This structure is shown schematically on the right (including an arbitrarily-placed H atom) together with the structural parameter values, including small perpendicular and parallel shifts of the Cu atoms, bonded to the carboxylate, relative to the ideally-located Cu(110) surface atoms.

of the COO and C=O oxygen atoms are also rather weak, but particularly near normal emission there is clearly an underlying long-period modulation. This long period indicates that the scattering path-length difference is reasonably short, while the fact that the modulations are strongest at normal emission suggests that the O atoms giving rise to these modulations lie close to atop Cu surface atoms, thus giving rise to scattering in the generally favoured 180° backscattering angle. However, while the COO oxygen atoms contribute to a clear long-period modulation, the emission from the C=O oxygen atom is expected to contribute only weak modulations, like that observed from the OH species. The consequential damping of the PhD modulations will, at least in part, account for the relatively weak amplitude of the modulations (less than ±10%) observed even at normal emission.

This interpretation is confirmed and quantified by the results of multiple scattering simulations for a range of possible adsorption sites, Cu–O bond-lengths, molecular twists and tilts, local surface relaxations, and vibrational amplitudes of the emitter and scatterer atoms. Identifying the best-fit structure over such a search is aided by the use of an objective reliability- or *R*-factor defined as a normalised sum of the squared differences between the theoretical and experimental modulation amplitudes $R = \Sigma(\chi_{th} - \chi_{ex})^2/\Sigma(\chi_{th}{}^2 + \chi_{ex}{}^2)$. The structural model yielding the lowest value of *R* is identified as the best-fit structure. Fig. 8 shows a comparison of a subset of the experimental COO + C=O O 1s PhD spectra (taken from the complete set shown in Fig. 7, mostly for small polar angles for which the modulations are strongest) with the results of multiple scattering simulations for the best-fit structural model, with an associated value of *R* of 0.40. This relatively high value (*R* values of 0.2 or less can be achieved for some adsorbate systems) reflects the fact that all modulations are rather weak and so the relative level of the noise is quite high. This structure is also shown schematically in Fig. 8 together with the best-fit structural parameter values (the OH hydrogen atom is shown for completeness but its location cannot be obtained from a PhD study due to its weak scattering cross-section). The local bonding geometry is equivalent to that of the formate, acetate, benzoate and mono-tartrate species on the Cu(110) surface; the molecule bridges two nearest-neighbour Cu atoms along the [001] azimuth with the bonding O atoms slightly off atop sites. This model is also consistent with the results of DFT calculations that find standing-up monooxalate species to be energetically favoured over a wide range of coverages [36]. The Cu–O nearest-neighbour bond length of the best-fit structure shown in Fig. 8 is 2.00 ± 0.04 Å, to be compared with the value found in the DFT-D2 calculations of 2.00 Å. More precisely, when intermolecular H-bonding is present the Cu–O distance of an O also engaged in the H-bond is 2.01 Å and shortens to 1.99 Å for the other O. These calculations indicate that the height difference of the carboxylate O and C atoms is 0.59 Å; O 1s PhD is relatively insensitive to this parameter, so the discrepancy with the theoretical value is not unreasonable.

4.3. Low-coverage phase

As the SXPS from the low-coverage lying-down dioxalate phase shows only a single O 1s peak, extracting the associated PhD spectra was straightforward. Unfortunately, identifying a structural model for which multiple scattering simulations gave a satisfactory fit to these data proved to be considerably more challenging despite running a vast number of calculations based on three-dimensional grid searches around a number of plausible starting models, but also running automated search routines from different starting points using the particle-swarm optimisation (PSO) method [44]. These procedures identify structures with the lowest *R*-factors in a multidimensional parameter hyperspace. Unfortunately, although this process did yield some structural models with values of *R* down to ~0.40, these models involved structural parameter values that were physically implausible - for example Cu–O nearest neighbour distances of ~2.30 Å or more, or of 1.6 Å or less.

Of course, the information from NEXAFS and SXPS provides some clear constraints on the likely structure. The single O 1s peaks in SXPS clearly indicates the species is fully deprotonated and NEXAFS shows the molecular plane is near-parallel to the surface, so it seems likely that all four O atoms bond to the Cu surface. On the other hand, the O 1s PhD modulations at normal emission are extremely weak (see Fig. 9), and do not show any clear dominant long-period modulations. This seems to indicate that the O atoms are *not* directly atop surface Cu atoms, as in the monooxalate species, and indeed as in all other carboxylates previously studied by PhD on Cu(110). Of course, the ability of a dicarboxylate to have all O atoms close to atop on Cu(110) depends on the matching of the O–O distances in the molecule and the Cu–Cu distances on the sur-

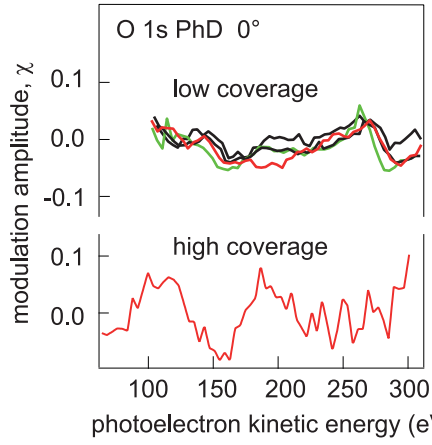

Fig. 9. Comparison of 4 individual O 1s PhD spectra recorded from the low coverage oxalate phase on Cu(110) with the representative spectrum in the same geometry from the high coverage phase (as shown in Figs. 7 and 8). The individual low-coverage spectra are recorded from different preparations and indicate the degree of reproducibility of the weak modulations.

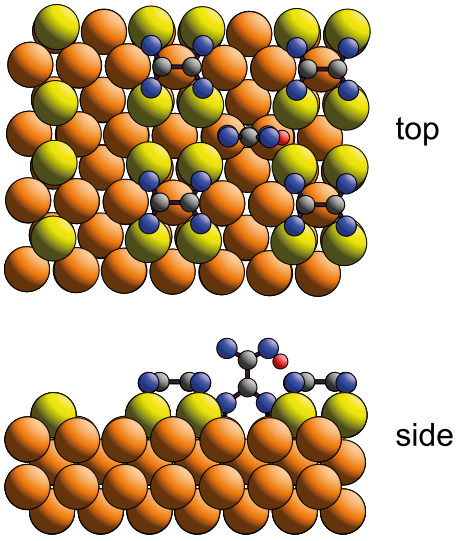

Fig. 10. Schematic model of a missing-row (3 × 2) phase formed by lying-down dioxalate species, showing that additional adsorption of standing-up monooxalate species would occupy sites at the centre of this mesh, potentially accounting for the 'defect' sites seen in the STM images of Figs. 3 and 4. For clarity the outermost Cu layer atoms are shown in a different colour from those of the underlying bulk. (For interpretation of the references to colour in this figure legend, the reader is referred to the web version of this article.)

face. In this regard, dioxalate lacks the flexibility of both the ditartrate species and the amino acids.

Weak modulations may in part arise from the fact that the PhD modulations come from an incoherent sum of the modulations from four different O atoms in the dioxalate; these four O atoms could have different local adsorption sites, although the two-fold symmetry of both the molecule and the substrate might reasonably be expected to lead to most O atoms occupying symmetrically-equivalent sites. Nevertheless, finding a model structure that shows such extremely weak modulations at normal emission proved difficult, while the generally weak modulations at all angles (and thus higher levels of noise relative to the modulations) necessarily leads to higher values of the *R*-factor even for the best models. This also results in weak variations of *R* in many regions of structural parameter hyperspace, rendering searches based only on identifying the lowest *R* values less effective.

There is, however, one further piece of information emerging from the STM data that may help to identify one important ingredient of the correct structural model. Specifically, the STM images of Figs. 3 and 4 provide evidence for a possible surface reconstruction associated with the low-coverage (3 × 2) phase. These images appear to show that some of the (3 × 2) unit meshes have molecules at their centres as well as at their corners, despite the fact that the centre and corner sites are inequivalent with respect to Cu(110) surface structure. In view of this it is unsurprising that the STM line scans at different bias potentials also indicate that these centred molecules differ in some way from those at the corners. Fig. 10 shows a model that could account for this effect. Specifically, if the (3 × 2) phase has every third [001] outermost layer Cu row missing, a standing up monooxalate species could bond to the exposed second layer Cu atoms in a site that lies at the centre of the mesh formed by the lying-down dioxalate species occupying high-symmetry sites on the double-Cu atom rows that are not missing. Of course, the O 1s SXP spectra from the low-coverage phase indicate the presence of very little, if any, standing-up monooxalate in the surface preparations from which PhD data were measured. However, the STM images of the defected (3 × 2) phase may be taken to provide us with evidence that these missing rows are a characteristic of a perfectly ordered (3 × 2) phase.

To explore this idea of a missing row model of the (3 × 2) dioxalate phase, further searches of possible structures based on this substrate model, starting from different local adsorption sites and orientations, were undertaken using the PSO routine. As for the PSO searches of models on the unreconstructed surface, several optimised structures with low *R*-factors were found with Cu–O bondlengths that were physically unreasonably long or short, but one solution emerged that had a more plausible Cu–O nearest-neighbour bonding distance of 1.86 Å. This model, and a comparison of a subset of the experimental O 1s PhD spectra with simulations based on the same model, are shown in Fig. 11. Notice that the subset of spectra chosen for these calculations are mostly those with the strongest modulations, although the normal emission spectrum is also included; clearly the correct model should at least reproduce the lack of strong modulations(±5% or less) in this high-symmetry direction. The value of the *R*-factor obtained from the structure shown in Fig. 11 is 0.50, which is certainly rather high. Not surprisingly in view of this, visual inspection of the spectra shows clearly that the simulated spectra include a few modulations that are much larger than those of the experimental data. On the other hand, most of the experimental peak energies are reproduced quite well, and the simulations for the normal emission spectra do show extremely weak modulations over most of the energy range, a key feature of the experimental data.

Of course, another source of possible quantitative structural models is energy minimisation calculations using DFT. In fact the published DFT study of oxalic acid derivatives on Cu(110) [37] did consider possible structures formed by a flat-lying dioxalate on this surface but concluded that the adsorption energy was very significantly lower than that of the standing-up monooxalate and indeed that most possible adsorption sites did not lead to stable adsorption but rather dissociation into two CO_2 molecules.

New DFT-D2 calculations were performed for the missing row structure leading to two possible stable adsorption structures for dioxalate, one of which has a significantly lower energy than any adsorption structure on the unreconstructed surface. These are shown in Fig. 12 along with the values of the associated adsorption energy. Specifically, with the molecule lying above the double rows between the missing rows, but centred above a second layer Cu atom with the C–C molecular axis aligned along the $[1\bar{1}0]$ azimuth, the energy was found to be 171 meV lower than the equivalent site on the unreconstructured surface.

Evidently, the best-fit structure obtained for the missing row model obtained from the PhD analysis (Fig. 11) is qualitatively very similar to the lowest energy structure found in the DFT calculations (Fig. 12). However, inspection of the detailed structural parameter values shows some significant discrepancies. Using the standard procedure for estimating precision in the PhD technique, based on a formal treatment of the vari-

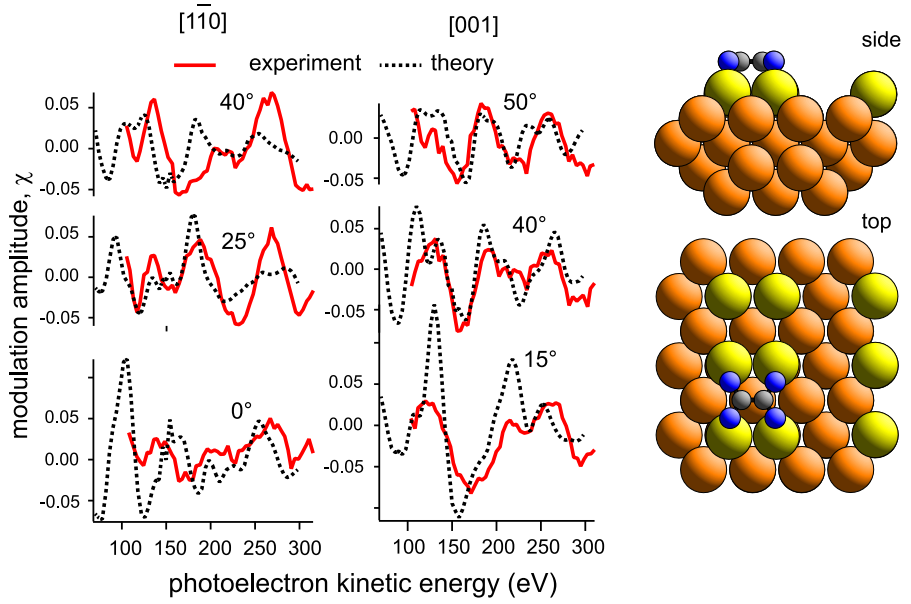

Fig. 11. Comparison of experimental and simulated O 1s PhD spectra recorded from the Cu(110)(3×2) dioxalate phase for the structural model illustrated on the right.

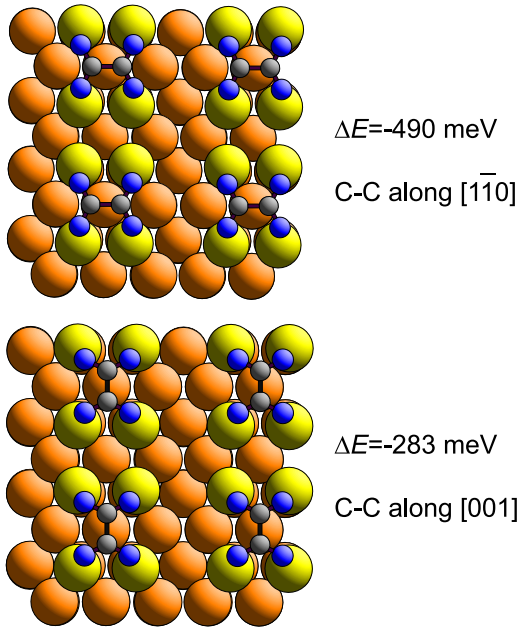

Fig. 12. Schematic top views of the two stable dioxalate adsorption geometries found in DFT calculations for the (3×2) missing row structure of Cu(110). For clarity the outermost Cu layer atoms are shown in a different colour from those of the underlying bulk. Also indicated are the calculated adsorption energies per molecule Δ*E*. (For interpretation of the references to colour in this figure legend, the reader is referred to the web version of this article.)

ation of the *R*-factor with changes to each structural parameter [6], we find the values of interatomic distances to be: Cu–O, 1.86 ± 0.06 Å; C–C, 1.15 ± 0.10 Å; C–O, 1.12(+0.21/−0.09) Å. For comparison the values of these parameters found in the DFT calculations are: Cu–O, 1.94 Å; C–C, 1.58 Å; C–O, 1.27 Å. Even bearing in mind the large error estimates in the precision of these PhD-derived values, there are significant quantitative differences between theory and experiment, despite the similarity in the qualitative structure in terms of local adsorbate-substrate registry and azimuthal orientation. Perhaps the most obvious problem with the experimentally-determined structural parameter values is the C–C distance that is unphysically short, even taking account of the limited precision. Of course, the O 1s PhD measurements are primarily sensitive to the relative location of the nearest-neighbour Cu atoms, which are more strongly scattering than C atoms and are also located at more favourable locations for backscattering. In this regard it is notable that the DFT calculations indicate significant lateral relaxations of the outermost layer Cu atoms, not only in the [1$\bar{1}$0] azimuth (into the space left by the missing row by 0.08 Å), but also along [001] by a larger value of 0.20 Å. Test simulations of the PhD spectra incorporating this large [001] shift (that was not tested in the original PSO search) by moving the O atoms to retain the same O–Cu nearest-neighbour registry led to an increase in the *R*-factor, and thus a less satisfactory agreement with the PhD experimental spectra

We therefore conclude that the PhD best-fit structure of Fig. 11 does represent a clear (local) *R*-factor minimum in parameter space that is qualitatively similar to the lowest energy structure found in the DFT calculations but does involve some significantly different structural parameter values, at least one of which (the C–C distance) is unphysical. There are almost certainly other local *R*-factor minima at other parameter values, but we have been unable to find one with realistic values of the parameter to which the O PhD is most sensitive, namely the Cu–O bondlength. Despite the unphysical C–C bondlength value, it seems extremely likely that this is the qualitatively correct structural model. The reasons underlying the failure of the PhD technique to provide a totally convincing final quantitative structural solution to this particular problem are unclear. The weak modulations and thus poorer signal-to-noise ratio are certainly a factor, and can be attributed to the fact that all the O atoms are in low symmetry sites, displaced by almost 1 Å from the ideal atop sites relative to surface Cu atoms. This contrasts with the situation for the standing-up phases of other carboxylic acids in which the O atoms are displaced from atop sites by only ~0.1 Å. Note that in searching for alternative structures that might provide a better fit to the PhD data a range of Cu adatom structures were also investigated; Cu adatoms have been suggested to play a role in a number of molecular adsorbate phases on copper surfaces including benzoate on Cu(110) [45]. Although some of these models were found to have total energies in DFT calculations comparable to that of the missing-row structure, none of these models led to an improved fit to the experimental data.

Of course, we cannot exclude the possibility that two or more coexistent adsorption geometries are present. Our STM images indicate that coadsorption of standing-up mono-oxalate species adsorbed onto the second layer at the missing row locations, can occur, but PhD sim-

ulations based on such a co-occupation model led to the best fit being found with zero occupation of this species. Moreover, the O 1s XPS data exclude any significant co-occupation of this standing-up species. It is also notable that the DFT calculations strongly suggest alternative adsorption sites of the dioxalate would be unstable.

5. Conclusions

The combination of (particularly O 1s) SXPS and O K-edge NEXAFS have provided clear evidence for two different adsorbed species on Cu(110) resulting from exposure to oxalic acid. At low coverages a doubly-deprotonated dioxalate species lies with its molecular plane approximately parallel to the surface, while at high coverages the adsorbate is a singly-deprotonated monooxalate with its molecular plane perpendicular to the surface lying in the $[1\bar{1}0]$ azimuth. STM and LEED show that the high coverage phase forms an ordered (3×2) structure, the implied coverage of 1/6 ML being consistent with SXPS data. STM images also show the presence of additional features, assumed to be extra oxalic acid-derived molecules, that occupy sites of the centre of the (3×2) unit mesh formed by the dioxalate species. Symmetry arguments clearly exclude the possibility that these additional molecules are dioxalate species at equivalent local sites, but the images could be consistent with the presence of missing [001] outermost layer Cu rows with monooxalate species bonded to second layer Cu atoms in the location of the missing rows.

O 1s PhD data from the high-coverage phase was found to be consistent with the monooxalate species bonded through the carboxylate O atoms in near-atop sites relative to nearest-neighbour surface atoms in the $[1\bar{1}0]$ rows. This local bonding geometry is equivalent to those of formate, acetate, benzoate and singly-deprotonated tartaric acid. Finding a model structure for the dioxalate on the unreconstructed Cu(110) surface from the O1s PhD data proved to be more challenging, at least in part due to the weak modulations, particularly near normal emission. However, DFT calculations, based on a reconstructed (3×2) surface, with every third [001] Cu surface layer row missing, as suggested by the presence of the centred unit mesh STM images, showed that the dioxalate bonds significantly more strongly to this surface. O 1s PhD simulations based on adsorption on this reconstructed surface identified a best-fit structural model qualitatively similar to that found to have the lowest energy in DFT calculations. Specifically, the molecule is found to occupy a hollow site on the Cu [001] double rows, directly above a second layer Cu atom, with the C–C axis along the $[1\bar{1}0]$ azimuth. However, some significant differences in structural parameter values are found between the DFT- and PhD-derived models, with at least one intramolecular bondlength (C–C) being unreasonably short in the PhD-derived model.

All data presented in this paper are available at http://wrap.warwick.ac.uk/94089.

Acknowledgements

The authors thank Diamond Light Source for access to beamline I09 (proposal number SI8436) that contributed to the results presented here. DAD would like to acknowledge funding from the Alexander von Humboldt Foundation. S.F. acknowledges the CINECA Award N.HP10CJCRO0, 2011 for the availability of high performance computing resources and support. G.C. acknowledges financial support from the EU through the European Research Council (ERC) Grant "VISUAL-MS" and from the EPSRC (EP/G043647/1).

References

[1] R. Han, F. Blobner, J. Bauer, D.A. Duncan, J.V. Barth, P. Feulner, F. Allegretti, Chem. Comm. 52 (2016) 9805.
[2] I.E. Wachs, R.J. Madix, J. Catal. 53 (1978) 208.
[3] D.S.Y. Ying, R.J. Madix, J. Catal. 61 (1980) 48.
[4] M. Bowker, R.J. Madix, Surf. Sci. 102 (1982) 542.
[5] B.A. Sexton, Surf. Sci. 88 (1979) 319.
[6] B.E. Hayden, K. Prince, D.P. Woodruff, A.M. Bradshaw, Surf. Sci. 133 (1983) 589.
[7] D.P. Woodruff, Surf. Sci. Rep. 62 (2007) 1.
[8] D.P. Woodruff, C.F. McConville, A.L.D. Kilcoyne, Th. Lindner, J. Somers, M. Surman, G. Paolucci, A.M. Bradshaw, Surf. Sci. 201 (1988) 228.
[9] D. Kreikemeyer-Lorenzo, W. Unterberger, D.A. Duncan, M.K. Bradley, T.J. Lerotholi, J. Robinson, D.P. Woodruff, Phys. Rev. Lett. 107 (2011) 046102.
[10] B.A. Sexton, Chem. Phys. Lett. 65 (1979) 469.
[11] M. Bowker, R.J. Madix, Appl. Surf. Sci. 8 (1981) 299.
[12] S. Bao, G. Liu, D.P. Woodruff, Surf. Sci. 203 (1988) 89.
[13] K-U. Weiss, R. Dippel, K-M. Schindler, P. Gardner, V. Fritzsche, A.M. Bradshaw, A.L.D. Kilcoyne, D.P. Woodruff, Phys. Rev. Lett. 69 (1992) 3196.
[14] B.G. Frederick, M.R. Ashton, N.V. Richardson, T.S. Jones, Surf. Sci. 292 (1993) 33.
[15] B.G. Frederick, F.M. Leibsle, S. Haq, N.V. Richardson, Surf. Rev. Lett. 3 (1996) 1523.
[16] B.G. Frederick, Q. Chen, F.M. Leibsle, M.B. Lee, K.J. Kitching, N.V. Richardson, Surf. Sci. 394 (1997) 1.
[17] M. Pascal, C.L.A. Lamont, M. Kittel, J.T. Hoeft, R. Terborg, M. Polcik, J.H. Kang, R. Toomes, D.P. Woodruff, Surf. Sci. 492 (2001) 285.
[18] J. Lee, O. Kuzmych, J.T. Yates Jr., Surf. Sci. 582 (2005) 117.
[19] C.C. Perry, S. Haq, B.G. Frederick, N.V. Richardson, Surf. Sci. 409 (1998) 512.
[20] Q. Chen, C.C. Perry, B.G. Frederick, P.W. Murray, S. Haq, N.V. Richardson, Surf. Sci. 446 (2000) 63.
[21] D.B. Dougherty, P. Maksymovych, J.T. Yates Jr., Surf. Sci. 600 (2006) 4484.
[22] S.M. Barlow, R. Raval, Surf. Sci. Rep. 50 (2003) 201.
[23] M. Ortega Lorenzo, S. Haq, T. Bertrams, P. Murray, R. Raval, C.J. Baddeley, J. Phys. Chem. B 103 (1999) 10661.
[24] B. Behzadi, S. Romer, R. Faseland, K-H. Ernst, J. Am. Chem. Soc. 126 (2004) 9176.
[25] V. Humblot, M.O. Lorenzo, C.J. Baddeley, S. Haq, R. Raval, J. Am. Chem. Soc. 126 (2004) 6460.
[26] C. Roth, D. Passerone, L. Merz, M. Parschau, K-H. Ernst, J. Phys. Chem. C. 115 (2011) 1240.
[27] Y. Wang, S. Fabris, T.W. White, F. Pagliuca, P. Moras, M. Papagno, D. Topwal, P. Sheverdyaeva, C. Carbone, M. Lingenfelder, T. Classen, K. Kern, G. Costantini, Chem. Commun. 48 (2012) 534.
[28] D.S. Martin, R.J. Cole, S. Haq, Phys. Rev. B 66 (2002) 155427.
[29] D.A. Duncan, W. Unterberger, D.C. Jackson, M.J. Knight, E.A. Kröger, K.A. Hogan, C.L.A. Lamont, T.J. Lerotholi, D.P. Woodruff, Surf. Sci. 606 (2012) 1435.
[30] J.-H. Kang, R.L. Toomes, M. Polcik, M. Kittel, J.-T Hoeft, V. Efstathiou, D.P. Woodruff, A.M. Bradshaw, J. Chem. Phys. 118 (2003) 6059.
[31] D.I. Sayago, M. Polcik, G. Nisbet, C.L.A. Lamont, D.P. Woodruff, Surf. Sci. 590 (2005) 76.
[32] C. Karageorgaki, K-H. Ernst, Chem. Comm. 50 (2014) 1814.
[33] C. Karageorgaki, D. Passerone, K-H. Ernst, Surf. Sci. 629 (2014) 75.
[34] D.S. Martin, R.J. Cole, S. Haq, Surf. Sci. 539 (2003) 171.
[35] M.N. Faraggi, C. Rogero, A. Arnau, M. Trelka, D. Écija, C. Isvoranu, J. Schnacht, C. Marti-Gastaldo, E. Coronado, J.M. Gallego, R. Otero, R. Miranda, J. Phys. Chem. C 115 (2011) 21177.
[36] S. Fortuna, Surf. Sci. 653 (2016) 41.
[37] S.J. Clark, M.D. Segall, C.J. Pickard, P.J. Hasnip, M.J. Probert, K. Refson, M.C. Payne, Z. Krist. 220 (2005) 567.
[38] Y. Yao, F. Zaera, Surf. Sci. 646 (2016) 37.
[39] A.F. Carley, P.R. Davies, G.G. Mariotti, Surf. Sci. 401 (1998) 400.
[40] S. Grimme, J. Comput. Chem. 27 (2006) 1787.
[41] J. Perdew, K. Burke, Y. Wang, Phys. Rev. B 54 (1996) 16533.
[42] S. Scandolo, P. Giannozzi, C. Cavazzoni, S. de Gironcoli, A. Pasquarello, S. Baroni, Z. Krist. 220 (2005) 574.
[43] P. Giannozzi, S. Baroni, N. Bonini, M. Calandra, R. Car, C. Cavazzoni, D. Ceresoli, G.L. Chiarotti, M. Cococcioni, I. Dabo, A. Dal Corso, S. de Gironcoli, S. Fabris, G. Fratesi, R. Gebauer, U. Gerstmann, C. Gougoussis, A. Kokalj, M. Lazzeri, L. Martin-Samos, N. Marzari, F. Mauri, R. Mazzarello, S. Paolini, A. Pasquarello, L. Paulatto, C. Sbraccia, S. Scandolo, G. Sclauzero, A.P. Seitsonen, A. Smogunov, P. Umari, R.M. Wentzcovitch, J. Phys. Cond. Mat. 21 (2009) 395502.
[44] D.A. Duncan, J.I.J. Choi, D.P. Woodruff, Surf. Sci. 606 (2012) 278.
[45] Q. Chen, C.C. Perry, B.G. Frederick, P.W. Murray, S. Haq, N.V. Richardson, Surf. Sci. 446 (2000) 63.